Charge injection into nanostructured TiO_2 electrodes from the photogenerated reduced form of a new Ru(II) polypyridine compound: the "anti-biomimetic" mechanism at work

Federico Ronconi,[†] Marie-Pierre Santoni,[‡] Francesco Nastasi,[‡] Giuseppe Bruno,[‡] Roberto Argazzi,[§] Serena Berardi,[†] Stefano Caramori,[†] Carlo A. Bignozzi,*[†] and Sebastiano Campagna.*[‡]*

† Department of Chemistry and Pharmaceutical Sciences, University of Ferrara, Via Fossato di Mortara 17-19, 44121, Ferrara, Italy.

§ CNR-ISOF co Department of Chemistry and Pharmaceutical Sciences, University of Ferrara, Via Fossato di Mortara 17-19, 44121, Ferrara, Italy.

‡ Department of Chemical, Biological, Pharmaceutical, and Environmental Sciences, University of Messina and Centro Interuniversitario per la Conversione Chimica dell'Energia Solare (SOLAR-CHEM), sezione di Messina, Via Stagno D'Alcontres 31, 98166 Messina, Italy

ABSTRACT

The charge transfer dynamics involving a new Ru(II) polypyridine complex (**1**), developed to generate highly oxidizing photoholes for water oxidation, was studied by electrochemical, photoelectrochemical and spectroscopic means. Mesoporous TiO_2 electrodes sensitized with complex **1**, under 1 sun illumination (420 nm cut-off filter) and a moderate applied bias (0.3 V vs. SCE), in ACN/0.1 M LiI as a sacrificial electron donor, reach anodic photocurrent of ~0.2 mA/cm^2 with 3% photon-to-current conversion efficiency. When 0.1 M aqueous sodium ascorbate (pH 3) is used instead of iodide, the photocurrent grows to ~0.7 mA/cm^2 and up to 1 mA/cm^2 if the concentration of ascorbate is increased to 0.5 M, explainable with a modification of the charge injection mechanism. This is the photoelectrochemical evidence, in the heterogeneous phase, of the so called "anti-biomimetic" pathway, confirmed in transient absorption spectroscopy by a long lived sharp bleaching at 480 nm and a narrow absorption between 500-550 nm, characteristic fingerprints of the photogenerated reduced state (**1**$^-$). After the formation of ***1**/TiO_2, the reductive quenching by ascorbate occurs, not observed in LiI where the classic oxidative quenching takes place. Due to the modest excited state oxidation potential, electron transfer onto TiO_2 is thermodynamically more favorable from **1**$^-$ rather than ***1**. Lastly, experiments performed with sensitized SnO_2 photoanodes, where ***1** undergoes the usual oxidative quenching, by charge transfer to the conduction band of the metal oxide, allowed to verify the interaction between **1**$^+$ and IrO_2 nanoparticles, grafted onto the surface, in order to drive photoinduced water oxidation.

INTRODUCTION

Photoinduced electron transfer from a molecular species grafted on a semiconductor is widely regarded as a possible first step in molecular artificial photosynthetic schemes aimed at the conversion of solar energy into chemical energy, based on Dye-Sensitized Photo-Electrosynthetic Cells (DSPEC). Significant examples of DSPEC have been reported in recent years, starting from pioneering approaches[1,2] and are now investigated by various research teams worldwide,[3-11] often in the form of half cells (i.e. photoanodes or photocathodes employed in three electrode configurations). Usually, the competition between interfacial recombination and hole transfer to a water oxidation catalyst is the key problem limiting the efficiency of such devices.[10]

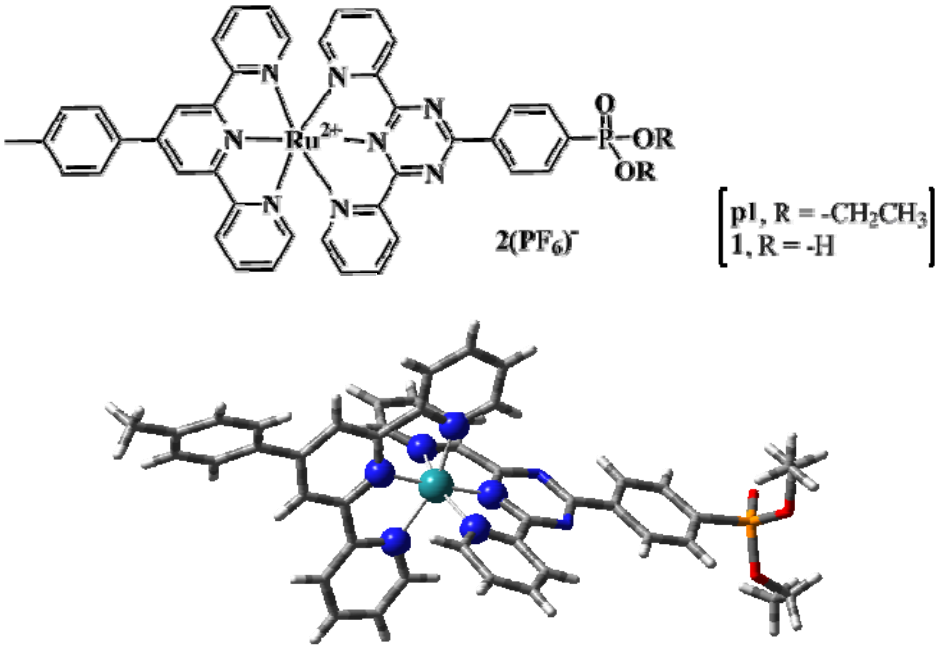

Figure 1. Above the structural formula of **p1** and **1**, below the $\mathbf{p1}^{2+}$ X-ray crystallographic structure (anions are omitted). Further X-ray crystallographic data are reported in the Supplementary Information. Full details are deposited at Cambridge Crystallographic Data Centre, deposition CCDC 1474484.

In the effort to develop a charge transfer sensitizer with a strongly oxidizing ground state, suited to be coupled with a wide selection of hole transfer catalysts (either nanoscopic or molecular species), we have developed and fully characterized compounds **p1** and the acidic form **1** (**Figure 1**). Interestingly, it was found that the excited state of the TiO_2-anchored species **1** has a poor ability to inject electrons into the TiO_2 conduction band (CB), whereas a substantial increase in photoanodic current is observed when the electrode is exposed to ascorbate solutions. This effect was interpreted on the basis of photoelectrochemical and transient spectroscopic measurements, according to the anti-biomimetic mechanism, (**Scheme 1**) where the main excited state deactivation pathway occurs via reductive photoinduced electron transfer by ascorbate salts, leading to the reduced Ru(II)-L^- species having an increased reduction potential.[12] Recently, the anti-biomimetic mechanism has been introduced to rationalize the machinery of a sacrificial system for photoinduced water oxidation, based on a tetranuclear dendritic Ru(II) species as the antenna/sensitizer and a tetraruthenium polyoxometalate species as the molecular catalyst, in the presence of persulfate salts, used as the sacrificial electron acceptor.[13-15] Some other authors[16,17] have previously considered this alternative pathway as a feasible approach to TiO_2 sensitization. Nevertheless, although spectroscopic evidence for charge injection by the reduced sensitizer was reported,[17] and sustained photocurrent generation on SnO_2 electrodes by such a mechanism was proposed to occur by Kirsch-De Mesmaeker,[16] a functional photoanode based on a nanostructured TiO_2 electrode taking clear advantage of the anti-biomimetic mechanism has remained elusive.[18-20]

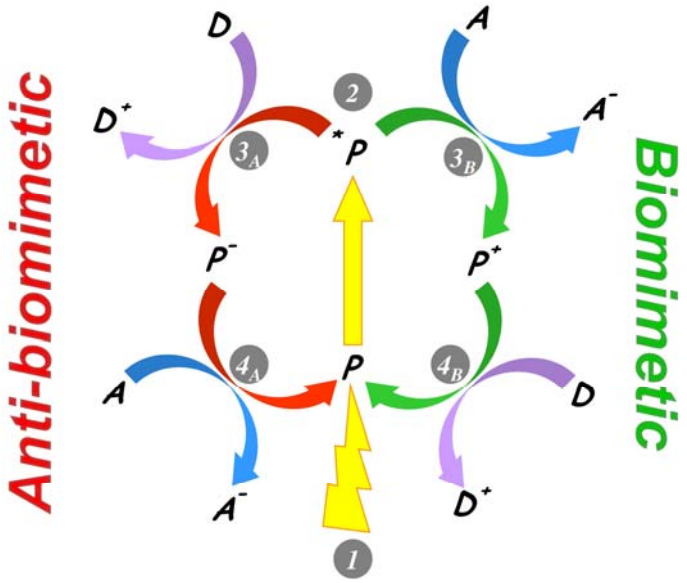

Scheme 1. Quenching of the excited state of a charge transfer photosensitizer (*P*): in the biomimetic pathway (green arrows, numbers 1-2-3_B-4_B) the oxidation quenching takes place by the electron acceptor (*A*, in our case the semiconductor CB), then the reductive quenching occurs by the electron donor (*D*, the electrolyte or the water oxidation catalyst) restoring the photosensitizer to the initial situation. Instead in the anti-biomimetic pathway (red arrows, numbers 1-2-3_A-4_A) the order of the quenchings is switched.

DSPEC, which are still at their infancy, are based on the biomimetic mechanism, although the anti-biomimetic mechanism could reserve intriguing properties: for example, it could allow to use as dyes for DSPECs (and the argument can be extended to Dye-Sensitized Solar Cells for solar-to-electricity conversion, DSSCs) even compounds whose excited states are not reducing enough to inject an electron into the semiconductor electrode, thus extending the range of useful species and removing some limits to the designing principles of these devices. Further, the anti-biomimetic pathway avoids the formation of the oxidized form of the photosensitizer, so it could be profitably used when stability of the oxidized photosensitizer – not an uncommon problem for DSSCs – is an issue.[21]

RESULTS AND DISCUSSION

Synthetic pathway, spectroscopic, photophysical and redox properties in solution

Our aim was to prepare a Ru(II) polypyridine compound having reversible electrochemistry, photochemical stability, and oxidation potential positive enough to drive water oxidation at mild pH, a necessary requirement for building a DSPEC suitable for water splitting.[22] These goals can be achieved by using chelating polypyridine ligands containing strong electron withdrawing substituents: as previously reported by some of us,[23] we envisaged that a Ru(II) compound like **1** would have been able to fulfil all these requirements. **Scheme 2** summarizes the synthetic pathways for ligand **L** and compound **1**, passing through the protected compound **p1**.

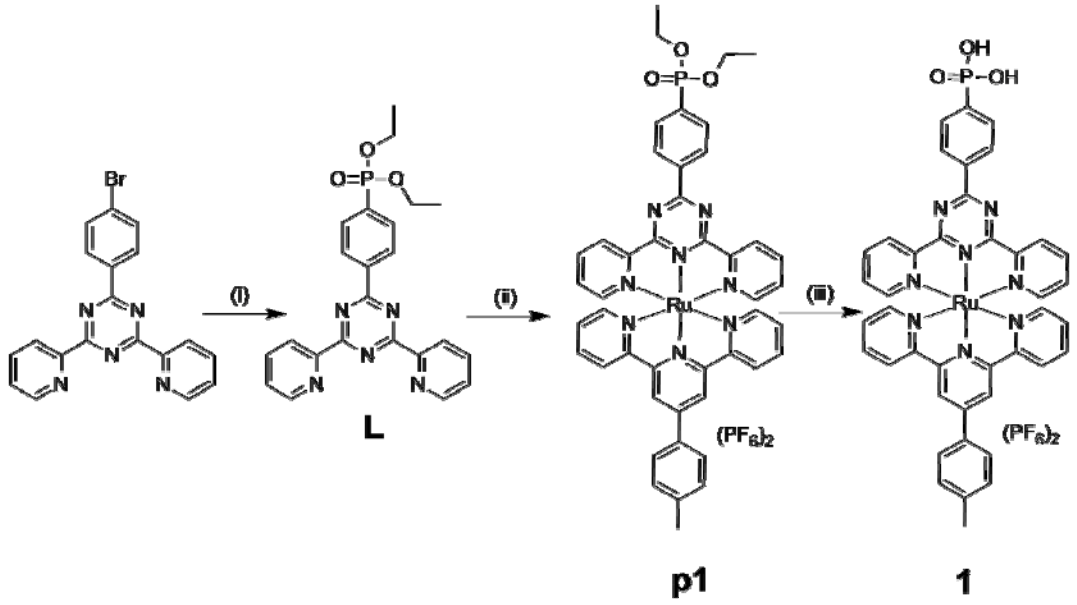

Scheme 2. Synthetic pathway for the new compounds **1** and **p1**. (i) $(dppf)PdCl_2$, toluene, NEt_3, $HP(OEt)_2$, 90 °C (yield 90%); (ii) $(Tol\text{-}tpy)RuCl_3$, $AgNO_3$, EtOH, reflux (yield 24%); (iii) 4 M HCl, reflux (yield 100%). dppf is 1,1-bis-(diphenylphosphino)ferrocene; Tol-tpy is 4'-(p-tolyl)-2,2':6',2''-terpyridine. The detailed procedures are reported in the Experimental Section.

The synthetic route is adapted from a previously reported procedure used for the synthesis of substituted bis(pyridyl)triazine ligands;[24] full details on the synthesis, characterization in

solution for both complexes, including mass spectrometry, proton, carbon (for complex **1**), and phosphorous NMR spectra, and X-ray crystal structure of **p1** are given in the Supporting Information.

The absorption spectra of **1** and **p1** in acetonitrile solution are shown in **Figure 2** and the relevant data are gathered in **Table 1**, where also the luminescence properties of the two compounds are reported (in acetonitrile fluid solution at room temperature and in butyronitrile rigid matrix at 77 K). The emission spectra at 298 K and 77 K of **p1** are also reported in the inset of **Figure 2**.

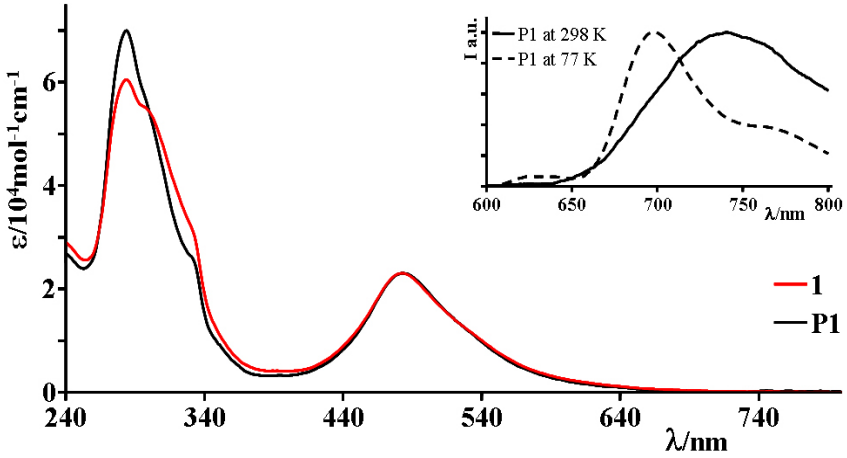

Figure 2. Absorption spectra of **1** and **p1** in acetonitrile solution. In the inset are shown the emission spectra of **p1**, both in acetonitrile solution at room temperature and in butyronitrile rigid matrix at 77 K.

The absorption and luminescence properties of **1** and **p1** are in line with the properties of Ru(II) polypyridine complexes in general,[25-27] and in good agreement with those of Ru(II) complexes containing bis(pyridyl)triazine ligands.[28] For both complexes, the absorption spectrum in the visible is dominated by spin-allowed metal-to-ligand charge-transfer (MLCT) bands and the emission spectra, both at room temperature and at 77 K, are assigned to triplet MLCT states, involving the bis(pyridyl)triazine ligand, which is expected to have a lower-lying π* orbital than the terpy-type ligand.[28] From the maximum of the **p1** emission spectrum

at 77 K (700 nm), a zero-to-zero spectroscopic energy (E^{0-0}) of 1.77 eV is obtained, which represents the energy gap between the triplet MLCT state and the ground state.

Table 1. Absorption spectra and luminescence properties of **1** and **p1**.

	Absorption[a]	*Luminescence, 298 K*[a]			*Luminescence, 77 K*[b]	
	λ/ nm (ε/ 10^4 M^{-1} cm^{-1})	λ/ nm	τ/ ns	Φ	λ/ nm	τ/ ns
p1	483 (2.28)	738	12	$< 10^{-4}$	700	630
1	482 (2.28)	722	7	$< 10^{-4}$	715	340

(a) In acetonitrile fluid solution. (b) In butyronitrile matrix.

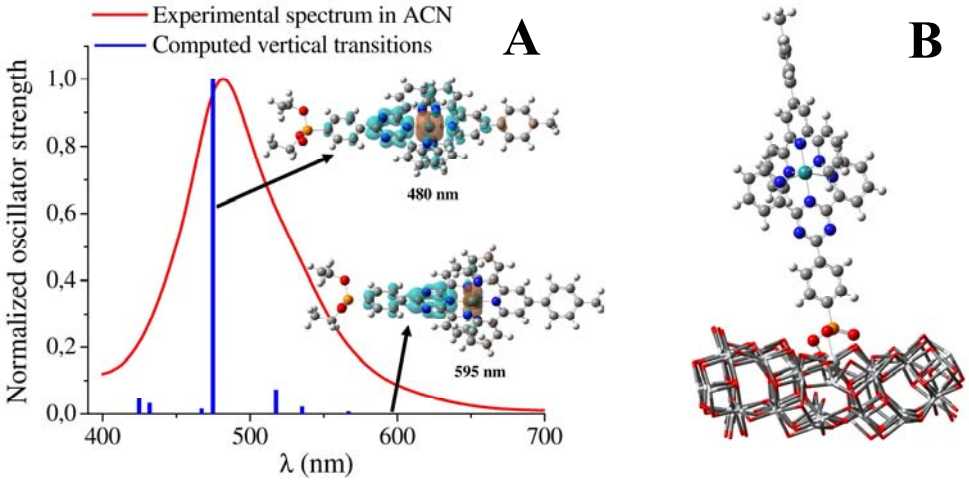

Figure 3. (**A**) Computed vertical transitions (blue lines) calculated at the TDDFT/LANL2DZ level compared with the experimental spectrum of **p1** in fluid acetonitrile solution (red line). The most significant transitions (lowest and most intense) are associated to EDDM maps (semitransparent surfaces) depicting "hole" (orange) and "electron" (cyan). (**B**) Complex **1** attached to the TiO_2 surface slab described at the MM level.

Time-dependent DFT (TDDFT) calculations carried out on the optimized ground state structure of **p1** in the presence of acetonitrile (ACN), described according to the Integral Equation Formalism of Polarizable Continuum Model (IEFCPM), predict singlet vertical

optical transitions which describe in a very satisfactory fashion the experimental spectrum measured in solution, showing a sharp absorption maximum at ca. 480 nm (**Figure 3A**). The computed transitions are generally characterized by a distinct MLCT character, involving the transfer of electron density from prevailingly Ru(II)-centered orbitals to the π* orbital of the bis(pyridyl)triazine (**L**) ligand. Interestingly, the aromatic ring bearing the phosphonic ester showed a dihedral angle close to 0°, in agreement with the X-ray results, (see **Figure 1**) as the consequence of stabilizing interactions between the triazole nitrogens and the protons of the phenyl ring bearing the phosphonic ester group. By contrast, the tilt angle of the tolyl substituent on the other terpyridine ligand is ca. 48°. The Electron Density Difference Maps (EDDM) show a sizable electron density on the ortho and para-position of the phenyl-phosphonic ring (**Figure 3A**), positions that should allow to establish an acceptable electronic coupling with the TiO_2 surface. However, contrary to carboxylic acid binding groups, no electron density is observed directly on the phosphonic group, in agreement with previous comparative studies on phosphonic acid functionalized MLCT complexes.[29] The MM (Molecular Mechanics) evaluation of the adsorption geometry of **1** on the 101 surface of a TiO_2 cluster, by relaxing only the two P-O-Ti linkages, while freezing the other internal coordinates, computed at a more accurate DFT level, show that **1** interacts with the TiO_2 surface with a tilt angle close to 80° (**Figure 3B**). Given this geometry, the shortest pathway for the electron transfer from the MLCT state to TiO_2 should involve a "through bond" mechanism with the mediation of non conjugating -PO_3H_2 group.

The very small emission quantum yield ($< 10^{-4}$) and short lifetime (ca. 10 ns) of **p1** and **1** at room temperature are attributed to the weak ligand field induced by the bis(pyridyl)triazine ligand, as consequences of both the tridentate nature of the ligands[25-27] and the inherent weak ligand field of the triazine subunit.[28] The difference between **p1** and **1** is minimal from a spectroscopic viewpoint (both absorption spectra and emission spectra are similar for the two

compounds (**Table 1**). On the contrary, a somehow larger difference in emission lifetime is found at 77 K, with that of **1** (340 ns) significantly shorter than that of **p1** (630 ns) in these conditions; possible radiationless pathways involving peripheral -PO_3H_2 groups (that are present in **1**, but not in **p1**) can have a role in determining this difference in these conditions.

Table 2. Redox properties of 1 and p1 in solution and on SnO_2 substrate (V vs. SCE).

	$E_{1/2}$ (ox)	*$E_{1/2}$ (red)*	*experimental conditions*
p1	+1.41	-0.71; -1.50; -1.61.	In ACN solution
1	+1.37		On TiO_2 electrode, in ACN/0.1 M $LiClO_4$
1	+1.32		On SnO_2 electrode, in ACN/0.1 M $LiClO_4$

The redox behavior of **p1** has been studied in acetonitrile by cyclic voltammetry (see Supplementary Information **Figure S1**; data are collected in **Table 2**) in the potential window +1.70/-1.80 V vs. SCE. The compound undergoes a reversible, one-electron oxidation process, involving the metal center, at +1.41 V vs. SCE, and several reversible one-electron reduction processes at -0.71 V, -1.50 V, and -1.61 V vs. SCE, that are assigned to first reduction of the bis(pyridyl)triazine ligand, first reduction of the terpyridine-type ligand, and second reduction of the bis(pyridyl)triazine ligand respectively. Such assignments are based on literature data of similar compounds.[25,28] The experimental electrochemical gap (2.12 eV) is in very good agreement with the computational spectroscopic gap (2.08 eV, from the lowest singlet transition energy at 595 nm), so confirming the identity between spectroscopic and redox orbitals and the presence of substantially localized redox states (i.e. states centered on distinct weakly interacting metal and ligand orbitals). The weak adsorption tail extending

further to the red, up to 700 nm could be thus originated by spin forbidden singlet to triplet absorption, consistent with the threshold (ca. 640 nm) of the emission spectra from the lowest triplet state.[25-27]

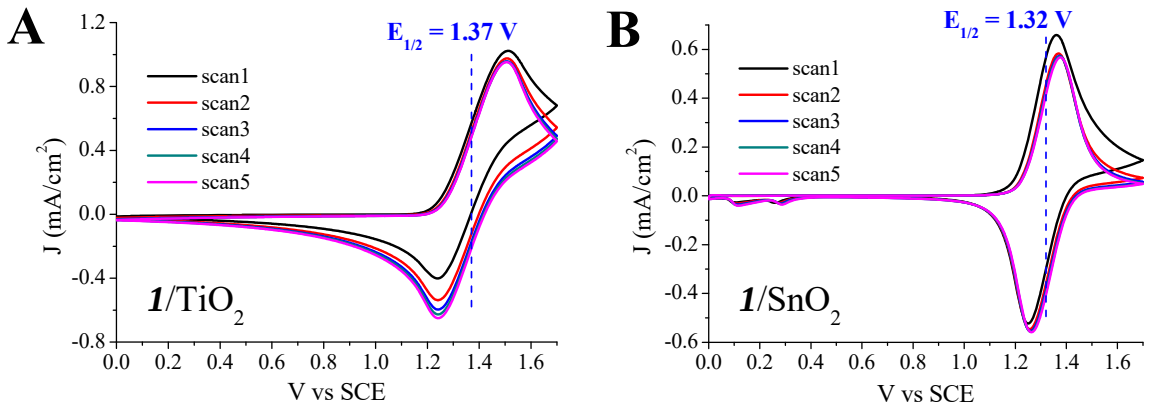

Figure 4. Cyclic voltammograms in ACN/0.1 M $LiClO_4$ of **1** on TiO_2 (**A**) and on SnO_2 (**B**) electrodes (scan rate = 50 mV/s).

The redox behavior of **1** in fluid solution could not be studied in detail: in fact, particularly on reduction, **1** tends to be absorbed on the electrode and a clear determination of the redox processes becomes impossible. Nevertheless **p1** represents a good model for the dye when anchored on TiO_2, and we also use the photophysical data of **p1** as a model for the properties of **1** anchored to TiO_2. Cyclic voltammetries in oxidative regime of **1** adsorbed either onto mesoporous TiO_2 or SnO_2 thin films are shown in **Figure 4**, confirming the reversible behavior observed in solution (**Table 2**). However, the metal-centered redox wave is slightly cathodically shifted (1.37 V vs. SCE on TiO_2 and 1.32 V vs. SCE on SnO_2) compared to the solution (1.41 V vs. SCE). Nevertheless the driving force is, in principle, still sufficient for the activation of a wide selection of water oxidation catalysts.[1,30-34]

From the luminescence data in **Table 1**, the redox data discussed above, and the simplified equation $^*E_{ox} = E_{ox} - E^{0\text{-}0}$,[35] commonly used to estimate the excited-state oxidation potential $^*E_{ox}$, for **p1**, the model for **1** anchored on TiO_2, $^*E_{ox}$ results to be -0.36 V vs. SCE for the

excited triplet state, indicating that photo-injection from the lowest excited state of **1** to the conduction band edge should be thermodynamically uphill.[36,37] The singlet excited state oxidation potential, estimated by combining the experimental E_{ox} with the computed singlet E^{0-0}, is more reducing, at a value of -0.66 V vs. SCE, approximately isoergonic with the conduction band edge of TiO_2 in non anhydrous acetonitrile, and barely above the conduction band edge of TiO_2 in aqueous solution at pH 3, according to V_{fb}= -0.4 – 0.06 × pH (V vs. SCE).[38] These values are definitely too low to allow for efficient photoinduced electron transfer from the excited state of **1** into the TiO_2 conduction band, particularly if the intersystem crossing to the triplet state is competing efficiently with injection from the singlet state. This is probably the case of complex **1**, given both insufficient driving force and non optimal coupling with the TiO_2 surface, due to the presence of non conjugating phosphonic binding groups. On the contrary, the **1** triplet excited state reduction potential ($^*E_{red}$ = +1.06 V vs. SCE), calculated from $E_{red} + E^{0-0}$,[25] is positive enough to allow for reductive excited state quenching from ascorbate.[39,40]

Photoelectrochemistry

Photoelectrochemical experiments, relevant to the discussion of the different excited state quenching pathways of **1**, were carried out with three different types of electrolytes: aqueous 0.1 M $NaClO_4$ at pH 3, aqueous sodium ascorbate at pH 3 where the ascorbate concentration ranged from 0.1 to 0.5 M and LiI in acetonitrile where the LiI concentration varied from 0.1 to 0.5 M.

The charge-transfer dynamics of **1**, relevant to application in molecular artificial photosynthesis, were preliminarily studied by fabricating transparent TiO_2 photoanodes with 7±1 μm thickness, according to the procedure reported in the experimental section. Soaking

in a 8×10^{-5} M acetonitrile solution of complex **1** at 50 °C for two hours leads to the functionalization of TiO_2 electrodes with maximum absorbance values of ~2 at 480 nm (**Figure 5A**), demonstrating efficient dye uptake. The assessment of the dye stability in aqueous solution at pH 3 in the presence of sodium ascorbate as sacrificial agent results in the loss of ca. 32% of the maximum optical density after ca. 10 minutes soaking (**Figure 5B**, red line), during which the photoelectrode is subjected to several J-V cycles (typically from +0.35 to -0.5 V SCE), until reaching a stationary photoelectrochemical response in J-V mode under illumination. By contrast, the stability in organic solvents under the same measurement conditions are optimal, with no appreciable changes in film absorbance during potential cycling (**Figure 5B**, dark cyan line). The bare TiO_2 films show, after 10 minutes soaking and potential cycling in 0.1 M ascorbate at pH 3, an absorbance increase in the blue region of the visible spectrum, due to the formation of a charge transfer adduct between surface exposed Ti(IV) and ascorbate (**Figure 5B**, dashed grey line) which was found to act as the charge transfer sensitizer.[41]

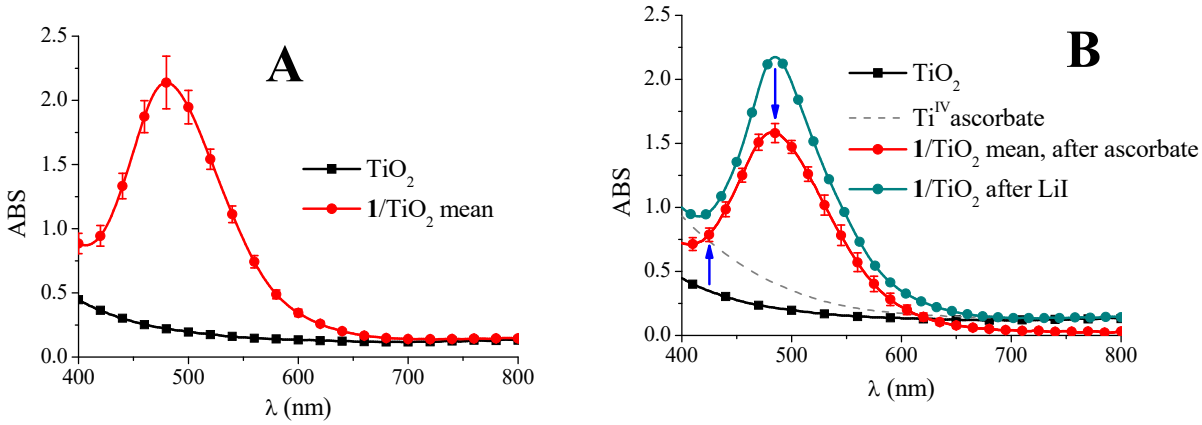

Figure 5. Averaged absorption spectra of the TiO_2 electrodes with error bars calculated on a set of three equivalent electrodes sensitized with **1**. (**A**) Before measurements, **1**/TiO_2 (red circles) in comparison with bare mesoporous TiO_2 (black squares). (**B**) Bare TiO_2 (black squares) compared with **1**/TiO_2 after a 10 minute measurement cycle in 0.1 M sodium ascorbate at pH 3 (red circles) and with **1**/TiO_2 after soaking and measurement in 0.1 M LiI in ACN (dark cyan circles). The absorbance of

the bare TiO_2 film immersed in 0.1 M ascorbate at pH 3 (dashed grey line) is also reported for reference.

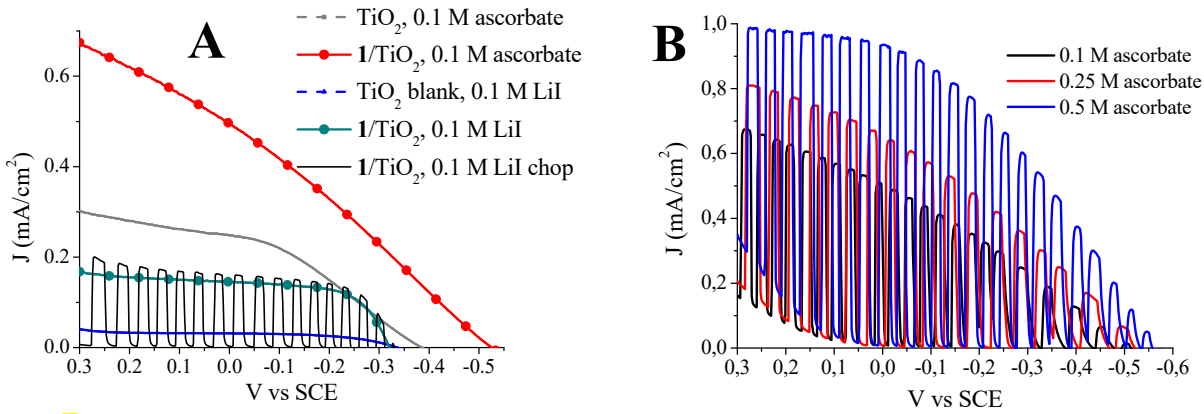

Figure 6. J-V curves of TiO_2 photoanodes in the presence of different electrolytes: (**A**) **1**/TiO_2 in 0.1 M ascorbate at pH 3 (red); 1/TiO2 in ACN/0.1 M LiI (dark cyan); bare TiO2 in 0.1 M ascorbate at pH 3 (grey); bare TiO_2 in 0.1 M LiI (blue); (**B**) Shuttered J-Vs of **1**/TiO_2 in the presence of increasing ascorbate concentration, 0.1 M (black) 0.25 M (red) 0.5 M (blue).

The J-V curves (**Figure 6A**) obtained under AM 1.5 G illumination with a 420 nm cut-off filter indicate that **1**/TiO_2 generates a modest plateau photocurrent density of ~0.2 mA/cm^2 and a V_{oc} of ca. -0.35 V vs. SCE in presence of 0.1 M LiI in acetonitrile. As expected blank TiO_2 electrode gave a negligible photoresponse, due to the insufficient light harvesting. By contrast, in 0.1 M sodium ascorbate at pH 3 a more than threefold increase in photocurrent (0.7 mA/cm^2) and enhanced photovoltage (-0.5 V vs. SCE) were observed for **1**/TiO_2 (**Figure 6A**). The blank TiO_2 film also generated a higher plateau photocurrent (0.3 mA/cm^2) due to the local formation of the titanium ascorbate sensitizer. Clearly, the formation of Ti(IV) ascorbate cannot explain the enhanced photocurrent observed with **1**/TiO_2, for the screening effect of the absorbed dye on TiO_2. Both photocurrent and photovoltage are improved by increasing the ascorbate concentration up to 0.5 M (**Figure 6B**), leading to rectangular-shaped phototransients reaching 1 mA/cm^2 and to a photovoltage of ca. -0.55 V vs. SCE, in good agreement with the estimation of the TiO_2 flat band potential.[38] Control experiments

carried out with **1**/TiO_2 in aqueous $NaClO_4$ at pH 3 (**Figure S2**) confirmed, through the observation of short lived photoinjection spikes reaching maximum amplitudes of only 2-3 $\mu A/cm^2$, the inefficient oxidative quenching of **1** loaded on TiO_2. Although, in the absence of an electron donor with facile kinetics, the low photocurrent is also determined by fast charge recombination with the oxidized dye, much stronger (50-100 $\mu A/cm^2$) injection transients are usually observed when charge injection is efficient.[42] It should be noted that, as previously documented,[4] photoelectrochemical experiments in the presence of iodide salts in aqueous solvents are scarcely meaningful due efficient adsorption of the iodide oxidation products on the sensitized TiO_2 surface, resulting in accelerated electron recombination via surface adsorbed poli-iodides.

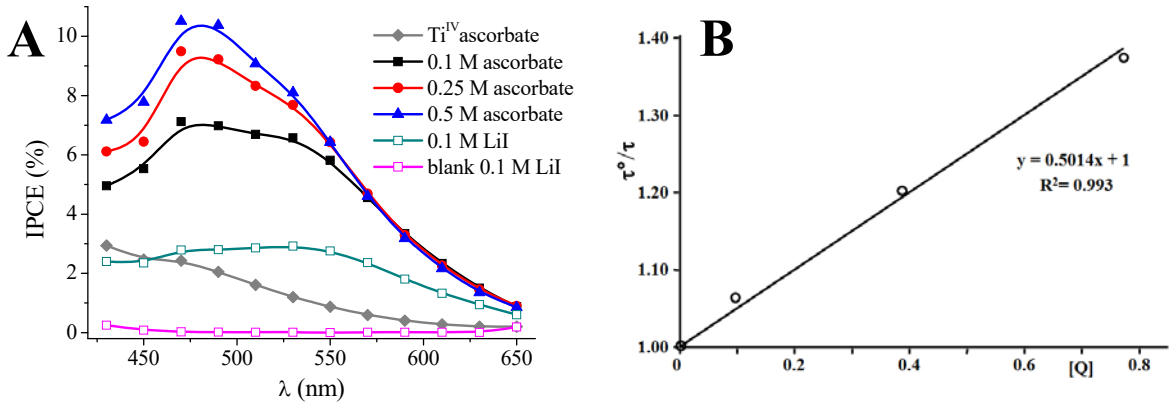

Figure 7. (**A**) Incident photon-to-current efficiency (IPCE) spectra of TiO_2 photoanodes in the presence of different electron donating electrolytes at 0 V vs. SCE: **1**/TiO_2 in the presence of different ascorbate concentration (0.1-0.5 M, from black to blue); **1**/TiO_2 in 0.1 M LiI in ACN (dark cyan); blank TiO_2 in 0.1 M ascorbate at pH 3 (grey); blank TiO_2 in 0.1 M LiI in ACN (magenta). (**B**) Stern-Volmer plot of the emission lifetime quenching of **1** in acetonitrile upon ascorbate addition. The ascorbate quencher solution was prepared in water (pH 3), for solubility reasons. Noteworthy, addition of LiI to a solution **1** in analogous conditions does not cause any emission quenching.

These results are consistent with IPCE spectra (**Figure 7A**), where the best conversion efficiency of ca. 10% is observed, within the explored conditions, in 0.5 M ascorbate. The IPCE spectrum of **1** in the presence of ascorbate shows a shoulder around 450 nm due to the

direct contribution of Ti(IV) ascorbate whose absorption begins to rise in this spectral region (**Figure 5B**, grey line). Nevertheless, the increased IPCE at 550 nm, in a region where direct contribution of Ti(IV) ascorbate becomes relatively unimportant, confirms that most of the photoconversion is originated by the ruthenium sensitizer. In the presence of LiI the IPCE is modest, confirming the poor reducing ability of the excited states of **1**, which combined to its short lifetime and to less than ideal electronic coupling with the TiO_2 surface, results in quantum yield of charge injection of the order of 3%, under the reasonable assumption that regeneration of **1** by iodide occurs with nearly unitary efficiency.

In order to further support our hypothesis, bimolecular electron transfer quenching of the luminescence of **1** by ascorbate was studied changing ascorbate concentration in acetonitrile solution. **Figure 7B** shows the typical, linear Stern-Volmer plot obtained, so confirming that ascorbate can efficiently quench the excited state of **1**, with a $k_q = 7.14\times10^7\ M^{-1}s^{-1}$.

Charge injection from the excited state of **1** in the presence of 0.1 M LiI is clearly observed on mesoporous SnO_2 films having < 2 μm thickness (maximum optical density 0.5, **Figure S3**), where the flat potential of SnO_2 (ca -0.1 V vs. SCE) clearly allows for the oxidative quenching of the excited state of **1**. The photocurrent, as well as the IPCE, increases by increasing the LiI concentration from 0.1 to 0.5 M with top values of 2.3 mA/cm^2 at 0.3 V vs. SCE, corresponding to a maximum IPCE of the order of 22% (**Figures 8A** and **8B**). The poor fill factor (ca. 0.25) observed with thin SnO_2 electrodes is ostensibly due to recombination from SnO_2 and from the underlying FTO back contact, which is more exposed to the electrolyte, being covered by a relatively thinner SnO_2 layer, if compared to the TiO_2 film. Monochromatic (490 nm) J-V curves (**Figure S4**) also show a more ideal shape under low power density, consistent with a small shunt resistance of SnO_2. From the described results, and taking into account the thermodynamic and electronic considerations mentioned above, it appears that, in the presence of LiI containing electrolytes, electron

injection into TiO_2 takes place directly from the excited state of **1**, following the usual oxidative quenching of the excited state of the sensitizer grafted on the semiconductor surface. However, it has a very modest efficiency on TiO_2 while it undergoes a significant improvement on SnO_2, due to increased exoergonicity for such charge transfer pathway.

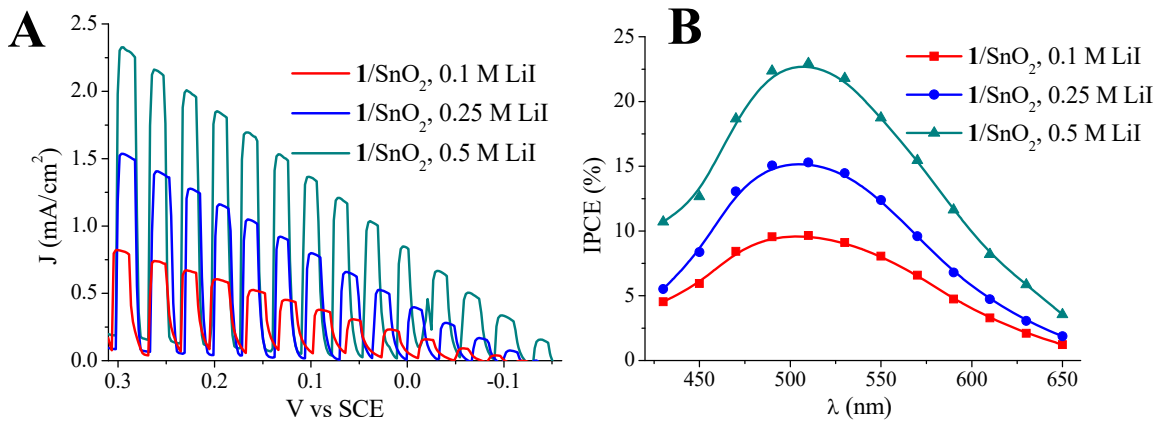

Figure 8. (**A**) J-V curves and (**B**) IPCE under 0.3 V vs. SCE potential bias of **1**/SnO_2 photoanodes evaluated in ACN solvent containing increasing concentration of LiI (from 0.1 to 0.5 M).

The ability to generate and store highly oxidizing photogenerated holes on SnO_2 photoanodes has been preliminarily confirmed in a water splitting cell, where **1** was coupled with IrO_2 nanoparticles acting as water oxidation catalyst.[2,11] Although the coupling between the sensitizer and the catalyst was not optimized, it can be observed (**Figure 9**) an increased photoanodic current density (from two times to three times higher current density under steady state conditions) in the presence of the IrO_2, suggesting the activation of hole transfer pathways to these co-adsorbed nanoparticles.

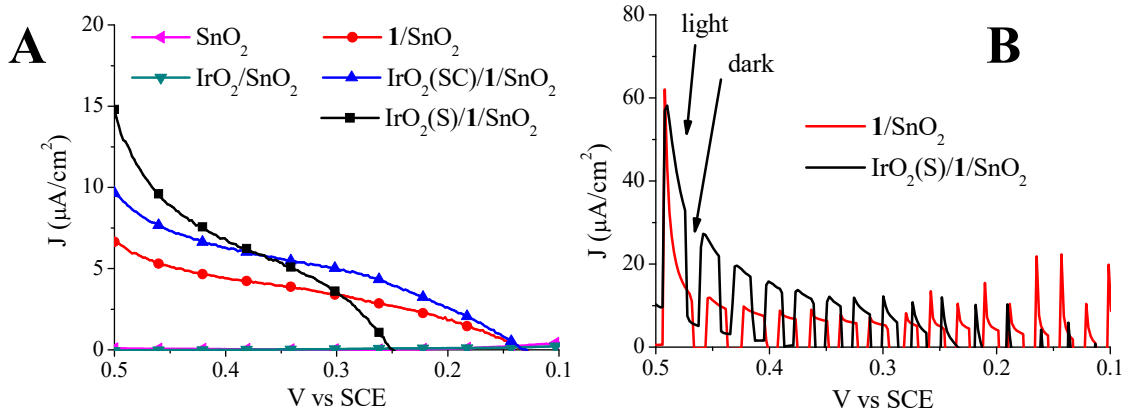

Figure 9. J-V curves, in aqueous pH 3 0.1 M $NaClO_4$, under continuous (**A**) and shuttered (**B**) illumination of **1**/SnO_2 in the presence of IrO_2 catalytic nanoparticles. Two different methods for casting IrO_2 particles on the photoanode were used: spin coating (SC, blue line) and soaking (S, black line).

The increased photon-to-electron conversion observed on TiO_2, in the presence of ascorbate salt, is consistent with a reductive quenching of the MLCT excited state due to bimolecular reaction with ascorbate, resulting in the formation of a species with a reducing ability higher than the singlet and the triplet excited states of **1**. The reductive quenching, i.e. the anti-biomimetic mechanism is followed by the thermodynamically-allowed electron injection into TiO_2. Transient absorption (TA) spectroscopy, in solution and on various semiconductor substrates, has been used to confirm this interesting point.

Transient Absorption Spectroscopy

Upon 532 nm laser excitation of **1** in acetonitrile solution, population of the triplet state occurs, which decays completely within 40 ns from the laser pulse, according to a monoexponential behavior with a lifetime of about 9 ns (**Figure 10**). This value appears to be in good agreement with that estimated by more accurate time-correlated single-photon-counting (TCSPC) technique (7 ns in fluid solution, **Table 1**), resulting in a transient absorption partly convoluted with the excitation profile of the Nd:YAG source (FWHM, 7

ns). The short-lived triplet state has the typical features of MLCT excited states of Ru(II) polypyridine complexes, characterized by the bleaching of the MLCT band, peaking at 480 nm, a relatively intense and narrow absorption in the blue region, peaking at ca. 400 nm, and by a weaker but well defined absorption band extending into the red with a broad maximum between 600 and 700 nm.

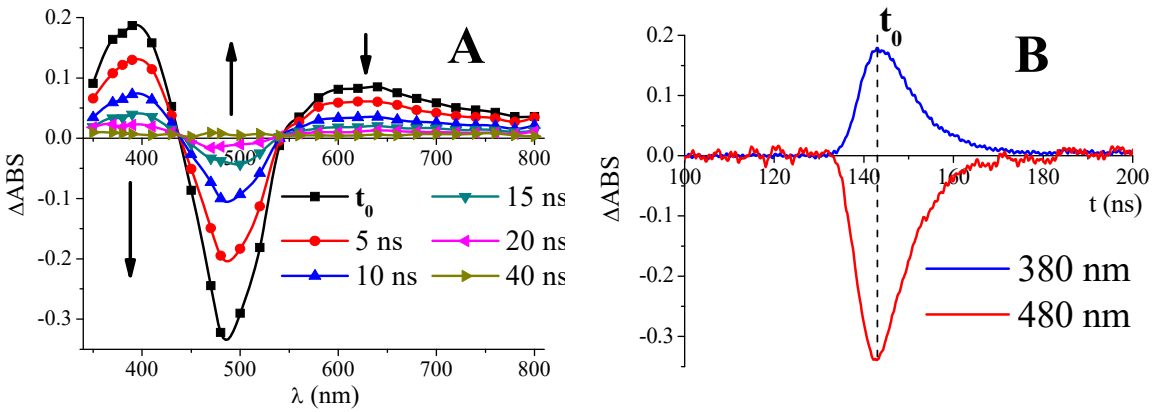

Figure 10. (**A**) Transient difference spectra of **1** in ACN solution upon 532 nm excitation; (**B**) Excited state decay observed in correspondence of the most intense transitions: 480 nm bleaching and 380 nm absorption.

When an excess of aqueous ascorbate at pH 3 is added to the ACN solution, in order to achieve a ca. 0.3 M concentration in an Ar-purged ACN/H_2O mixture, a significant change in excited state decay occurs, showing the instrumental response limited decay (τ = 7.5 ns) to a long-lived signal having at least 1/3 of the initial ΔA amplitude and which remains essentially constant within a time interval of 500 ns (**Figure 11B**). This signal is consistent with formation of the reduced state of **1**, which is able to survive long in the absence of oxygen and of other electron scavengers in the solvent medium. The TA of the reduced form shows some analogy with the triplet excited state spectrum, but it is characterized by its own diagnostic fingerprints consisting in a narrower structured bleaching peaking at 480 nm, preceded and followed by two small shoulders at 450 nm and at 510 nm, which develops in a narrow absorption between 500 and 550 nm (**Figure 11A** and **C**). The absorption at longer

wavelengths, beyond 600 nm, is weak, flat and featureless. It is interesting to note that, in large part, these spectral features are already present in the transients taken immediately after the excitation pulse, and are very similar to those recorded after the establishment of the long-lived state which follows the initial fast decay (**Figure 11C**). We thus conclude that, in the presence of a large excess of ascorbic acid, similar in concentration to that used in the electrolyte for photoanode testing, the reductive quenching in solution is nearly instantaneous (for the temporal resolution of our spectrometer) and that the fast initial decay occurring within few ns is mostly due to electron/hole recombination within the bimolecular adduct (i.e. within the ion pair **1**$^{-}$/ascorbate^{+}), of which only a fraction is able to separate, finally yielding the long-lived charge separated species. Similar spectral fingerprints, as well as long lived kinetics, are found in **1** grafted on ZrO_2 film, showing that **1**$^{-}$ can be accumulated also on inert (with respect to charge injection) semiconductor surfaces, when exposed to ascorbate solutions (**Figure 11D**).

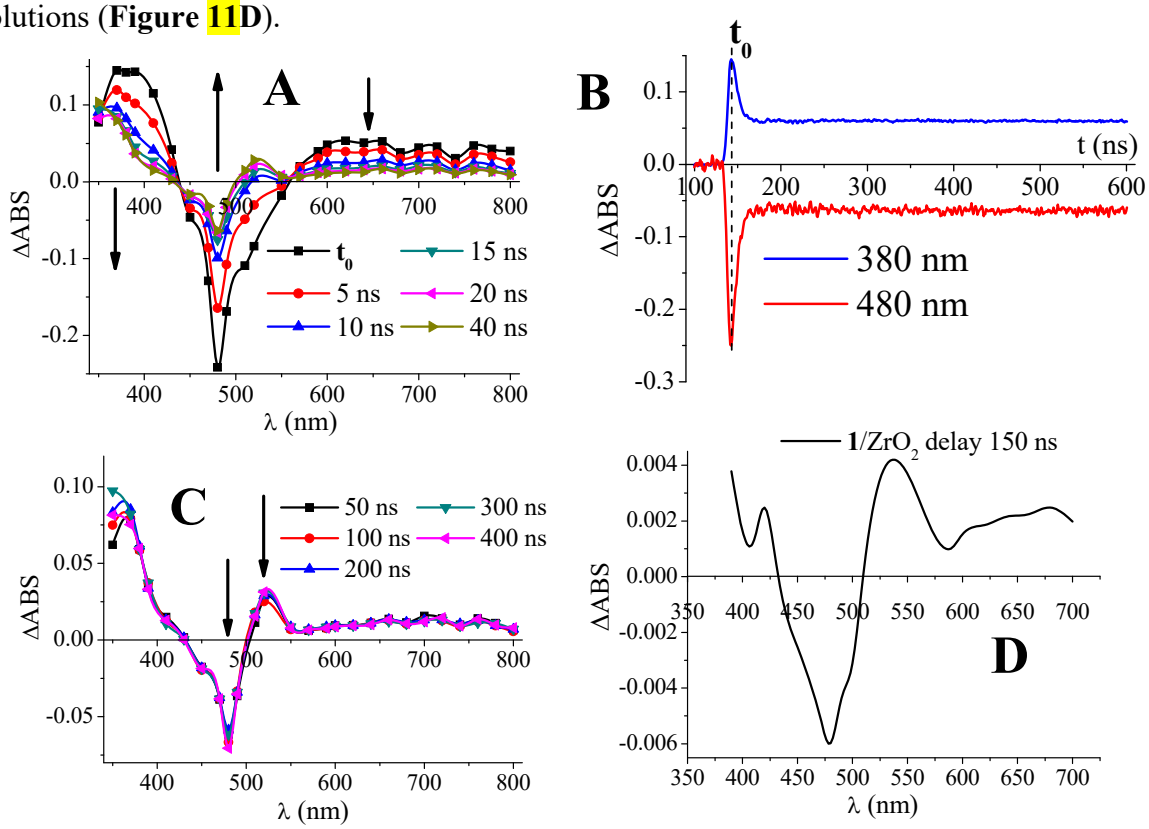

Figure 11. Transient difference spectra of **1** in the presence of ≈ 0.3 M sodium ascorbate in ACN/water mixture: transient difference spectrum (**A**) at early delays (0-40 ns) and (**C**) at longer

delays (50-400 ns), showing the achievement of a long lived state; (**B**) decay kinetics observed at 480 (bleaching) and at 380 nm (absorption); (**D**) transient difference spectrum recorded on ZrO_2 at long delays (150 ns) in order to avoid interference from the excited state.

The transient spectra of **1** loaded on SnO_2 exposed to ACN/0.1 M Li^+ solution are consistent with the formation of Ru(III), following the oxidative quenching of the excited state by charge injection into the SnO_2 conduction band. The $\mathbf{1}^+$ state is characterized by slow, multiexponential kinetics which do not completely lead back to the ground state on a time scale of 10000 ns (**Figure 12B**), according to the comparatively slow Ru(III)/e^-(SnO_2) back electron transfer. The characteristic spectral signature of the charge separated state $\mathbf{1}^+$/e^-(SnO_2) is summarized by the intense bleaching of the ground state, leading to a minimum at 480 nm followed by a 510 nm shoulder (**Figure 12A** for the 150-9000 ns time range and **Figure S5** for the early 0-150 ns time range). Contrary to the signature of the excited state, the transient spectrum of the oxidized sensitizer lacks the broad but well defined band having maximum between 650 and 700 nm and only shows a featureless, weak, sloping absorption rising for λ > 650 nm due to the sum of both LMCT transitions and of optical contributions of photoinjected electrons trapped into SnO_2.

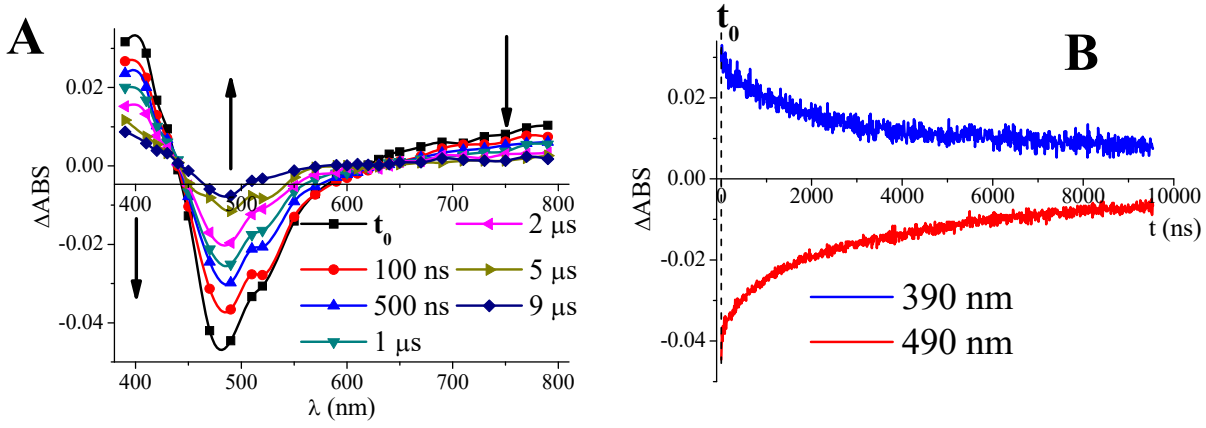

Figure 12. Transient spectrum of **1** loaded on SnO_2 thin films upon 532 excitations. (**A**) Transient difference spectrum recorded at 150-9000 ns delays after the excitation pulse. (**B**) Electron recombination kinetics observed at 490 nm (bleaching) and at 390 nm (absorption maximum).

The transient spectrum of **1** loaded on TiO_2 in the presence of ACN/Li^+ (**Figure 13A**) shows the dominating contribution of the triplet excited state of the sensitizer, decaying within few tens of nanoseconds and having the characteristic 650-700 nm absorption hump, confirming that excited state quenching by electron transfer into TiO_2 is largely inefficient. Nevertheless a small long lived amplitude having ca. 20% of the initial amplitude (**Figure 13B**) is detected and assigned, on the basis of the spectral fingerprints observed at long delays (i.e. bleaching band with two shoulders and sloping absorption for $\lambda > 650$ nm, **Figure S6**), to the (weakly efficient) formation of the oxidized dye. This is consistent with the small, but clearly detectable photoanodic current observed in ACN/0.1 M LiI (**Figure 6A**, dark cyan).

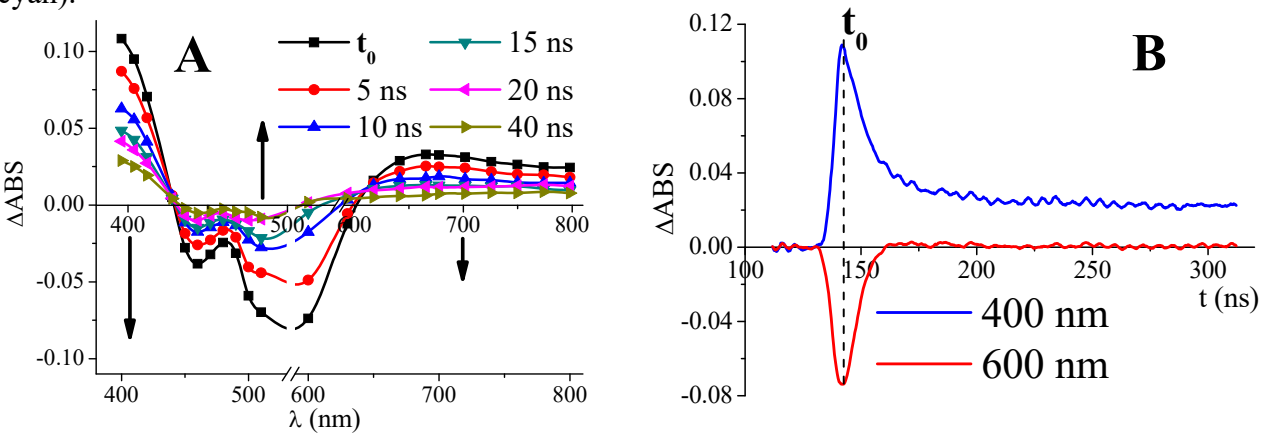

Figure 13. (**A**) Transient spectrum of **1** loaded on TiO_2 in the presence of ACN/0.1 M Li^+ electrolyte (0-50 ns delay); (**B**) kinetic traces observed at 600 and 400 nm, showing the formation of a long lived state assigned to Ru(III). At 600 nm the Ru(III) state has a negligible contribution and only the excited state decay is observed.

In the presence of sodium ascorbate at pH 3 (**Figure 14**) the dynamics on TiO_2 become complicated by the presence of at least three possible excited-state deactivation pathways, leading to three different transient species, all of them expected to have a short lifetime: a) the triplet excited state; b) the reduced state of the sensitizer (**1**$^-$), formed by reductive quenching of the excited state, which would be continuously depleted by charge transfer into

TiO_2 without possibility of substantial accumulation; c) the oxidized dye formed by injection from the singlet state, also short-lived due to reduction by ascorbate acting as electron donor towards Ru(III). The possibility to discriminate these three photo-products is related to the analysis of the transients at early delays: the spectral signature observed at 0-40 ns delays after the laser pulse is consistent with the prevailing presence of the triplet state of **1**, characterized by the structureless bleaching of the ground state followed by the diagnostic absorption band in the 650-700 nm interval. Consistent with the excited state lifetime measured in solution and on ZrO_2, 90% of the initial amplitude decays within 40 ns from the laser pulse. There is a small component, about 10% of the initial ΔA, which however survives well beyond the excited state decay. We note that, due to the convolution of the excited state with the excitation pulse we cannot reliably observe a shortening of the triplet lifetime in the presence of the reductive quenching by ascorbate.

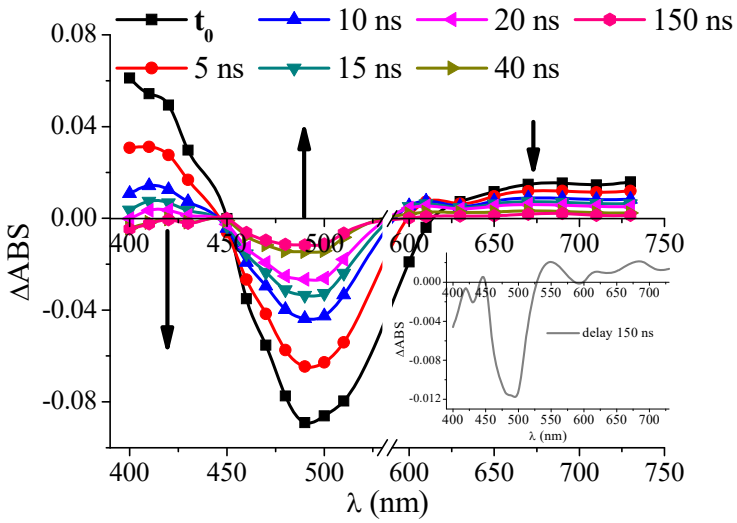

Figure 14. Transient absorption spectrum of **1** loaded on TiO_2 in the presence of 0.3 M ascorbate at pH 3: inset: transient spectrum recorded at 150 ns delay, after the complete decay of the excited state.

Despite the modest signal-to-noise ratio, the analysis of this residual component is consistent with the survival of a small population of $\mathbf{1}^-$, characterized by a narrow bleaching band centered at 480 nm and by a flat long wavelength absorption (**Figure 14**, inset), which,

contrary to the oxidized state, does not display the characteristic sloping feature for $\lambda > 700$ nm. Noteworthy, the TA spectrum of this residual component is similar to the TA spectrum related to **1** on ZrO_2 in the presence of ascorbate (in comparison **Figure 11D** and inset in **Figure 14**). Therefore, in the presence of ascorbate, the main sensitization mechanism involves reductive quenching of the excited state of **1**. The observation of a prevailing population of the excited state is suggestive of the following possibilities: (i) a significant fraction of the complex immobilized on the TiO_2 surface is not able to form encounter complexes with ascorbic acid contained in the electrolyte; (ii) a large fraction of $\mathbf{1}^-$ is able to inject within the instrumental response of the laser apparatus and is therefore not observed; (iii) a large fraction of the $\mathbf{1}^-$/ascorbate$^+$ adduct recombines reforming **1** at the triplet state. Based on the photoelectrochemical results, from which maximum IPCEs of the order of 10% are observed (**Figure 7A**), we can dismiss point (ii) otherwise much larger photon-to-electron conversion would be achieved. The possibility (iii) seems also unlikely, based on the results obtained in mixed ACN/water solution (**Figures 11A** and **11C**), considering that no prevailing triplet state is observed in those conditions, but rather the reduced state is the dominating species, already clearly observable at very early delays after the excitation pulse. We can thus confirm that in the presence of ascorbate salt, on the TiO_2 surface a non-negligible fraction of excited state of **1** is reductively intercepted by ascorbic acid, forming $\mathbf{1}^-$ as the main charge-injecting species. This process has, on TiO_2, a rather low efficiency, probably due to the limited availability of ascorbate, interacting mostly with the surface, as well as to steric blocking effects that limit the access of ascorbate to the majority of titania sites on the electrode, consistent with relatively modest IPCE. Nevertheless, in the case of the dye under investigation, it provides a significantly improved photon-to-electron conversion with respect to the conventional sensitization mechanism based on direct charge transfer to

TiO_2. We would like to note that the residual long-lived transient component associated to the persistence of $\mathbf{1}^-$ on TiO_2 is ostensibly due to a fraction of reduced dye, which is not able to inject due to the occupancy of surface sites having either a locally higher reorganization energy or less favorable electronic coupling with the surface. Fluctuations in the reorganization energy associated to the charge transfer may be decisive in determining the possibility of injection by weakly exoergonic states, like that of $\mathbf{1}^-$ compared to the CB level of TiO_2.

CONCLUSIONS

In conclusion, we have designed and synthesized a new phosphonated Ru(II) polypyridine complex, characterized by electrochemical reversibility, strongly oxidizing Ru(III) state, and intense optical transitions in the visible region, in order to obtain an efficient and stable dye for the sensitization of semiconductor based photoanodes in DSPEC. Preliminary spectroscopic and electrochemical analysis have underlined the promising properties of **1** as sensitizer, both for the high ε values in the visible region and the redox potentials. From ab-initio results and MM modelling of **1** grafted onto TiO_2 cluster surface, it was expected a less than ideal electronic communication between the dye MLCT state and TiO_2 acceptor states, due to a chemisorption geometry that constrains the charge transfer trough the non-conjugating PO_3H_2 groups.

The photoelectrochemical characteristics of **1**/TiO_2 electrodes, in ACN/0.1 M LiI, reflected the computational data, achieving an anodic photocurrent of ~0.2 mA/cm^2 with IPCE at 3%, consistent with the poorly reducing abilities of the lowest MLCT excited state of the dye. This limitation was circumvented by using SnO_2, where much larger photocurrents and IPCE

were observed, thanks to the increased charge injection driving force in the low lying SnO_2 CB. The ability to photogenerate and transfer h^+ to co-adsorbed WOC was also confirmed, by the significantly enhanced photoanodic response in the presence of IrO_2 NPs. Interestingly, the photocurrents on TiO_2 substrates were largely increased, compared to ACN/LiI, in the presence of aqueous pH 3 sodium ascorbate, with photocurrents undergoing a three to five fold enhancement depending on the concentration of ascorbate, with corresponding photon-to-current conversion between 7-10%; we have attributed this behavior to a modification in the charge injection mechanism. The anti-biomimetic pathway, confirmed by transient differential absorption spectra, allows for a more efficient electron transfer from $\mathbf{1}^-$ to the TiO_2 CB, thanks to both a stronger reduction potential and a longer lifetime of the active state.

Besides the fact that a non ambiguous evidence for the excited state reductive quenching occurrence on TiO_2 photoanodes was provided,[43,44] the possibility of exploiting such charge transfer pathway may result in some intriguing consequences, like the exploitation of sensitizer-catalyst ionic couples/assemblies where the high redox potential of the dye, necessary to activate the WOC, would impede injection of electron from the excited state into semiconductor. Thus the range of useful species for sensitization could be extended resulting in the removal of some constraint for dye and device design for solar water splitting. Moreover, the anti-biomimetic pathway can be useful when the oxidized form of the dye can affect the stability of the functionalized electrode, a non unusual case for DSSC (and DSPEC).

EXPERIMENTAL SECTION

Materials. LiI (99.999%) were from Alfa Aesar. Alconox®, lithium perchlorate ($LiClO_4$) ACS reagent ≥95.0%, ammonium hexafluorophosphate (NH_4PF_6) ≥95%, tetrabutylammonium hexafluorophosphate ($TBAPF_6$) purum ≥98.0%, silver nitrate ($AgNO_3$) ACS reagent ≥99.0%, anhydrous pellets sodium hydroxide (NaOH) reagent grade ≥98.0%, absolute ethanol (EtOH) puriss. p.a. ACS reagent ≥99.8%, anhydrous acetonitrile (ACN) 99.8%, ACS grade ≥99.8% 2-propanol, anhydrous toluene (TOL) 99.8%, anhydrous *N,N*-dimethylformamide (DMF) 99.8%, ascorbic acid 99% grade, perchloric acid ($HClO_4$) ACS reagent 70%, 37% hydrochloric acid (HCl), triethylamine (Et_3N) ≥99%, pyridine-2-carbaldehyde, 4-bromobenzaldehyde, [1,1-bis-(di-phenylphosphino)ferrocene]dichloropalladium(II), diethyl phosphite, 4-tolualdehyde, silica gel and the deuterated solvents were from Sigma Aldrich. 2,4-di(2'-pyridyl)-6-(*p*-bromophenyl)-1,3,5-triazine were synthesized according to previous literature reports,[24] as well as the ligand 4'-(tolyl)-2,2':6',2''-terpyridine (Tol-tpy)[45] and their Ru(III)Cl_3 complexes.[46] 18-NRT TiO_2 colloidal paste was purchased from Dyesol. SnO_2[11] and ZrO_2[47] colloidal pastes was prepared according to previously reported directions. Colloidal IrO_2 nanoparticles solution was prepared by following literature routes.[48] TEC 8 (8 Ω/) Fluorine Tin Oxide (FTO) 20×20 cm conductive glass slides were obtained from Pilkington. Dry solvents were kept in Schlenk flasks, under nitrogen, on activated molecular sieves. All reagents, unless otherwise stated, were used as received.

Synthesis of diethyl 4-(4,6-di(pyridin-2-yl)-1,3,5-triazin-2-yl)phenylphosphonate (L). The synthesis (**Figure S7**) was adapted from literature.[49] In a 50 ml round flask, 19 mg of [1,1-bis-(di-phenylphosphino)ferrocene]dichloropalladium(II) (MW = 735.90 g/mol, 0.026 mmol) were suspended in 5 ml of anhydrous toluene under N_2 and vigorous magnetic stirring. Successively 200 mg of 2,4-di(2'-pyridyl)-6-(*p*-bromophenyl)-1,3,5-triazine (MW =

390.24 g/mol, 0.51 mmol), 72 µl of diethyl phosphite (MW = 138.10 g/mol, ρ = 1.072 g/ml, 0.56 mmol) and 80 µl of NEt_3 (MW = 101.19 g/mol, ρ = 0.726 g/ml, 0.57 mmol) were added. The mixture was heated at 90 °C for 24 hours under N_2. The solution was cooled at room temperature and the solid was filtered off. The filtrate was evaporated to dryness to afford 206 mg of diethyl 4-(4,6-di(pyridin-2-yl)-1,3,5-triazin-2-yl)phenylphosphonate (MW = 447.43 g/mol, 0.46 mmol, 90% yield) as a yellow oil. ^{1}H (Chloroform-d_1, 300 MHz) δH (ppm): 8.97 (d, J = 6 Hz, 2H), 8.91-8.80 (m, 4H), 8.09-7.96 (m, 4H), 7.55 (m, 2H), 4.16 (m, 4H), 1.36 (m, 6H) (**Figure S8**). ^{31}P (Chloroform-d_1, 121 MHz) δP (ppm): 17.6, 17.5 (**Figure S9**). ESI-MS, m/z: [**L**+H]$^+$ calculated for $C_{23}H_{23}N_5O_3P$ 448.1533; found 448.1536 (I = 1 x 10^2 counts (%)) (**Figure S16**).

Synthesis of [Ru^{II}(tol-tpy)L](PF$_6$)$_2$ (p1 and 1). In a 100 ml round flask, 239 mg of (4'-(tolyl)-2,2':6',2''-terpyridine)Ru^{III}Cl$_3$ (MW = 530.82 g/mol, 0.45 mmol) and 229 mg of $AgNO_3$ (MW = 169.87 g/mol, 1.35 mmol) were refluxed for 1 hour in 15 ml degassed absolute EtOH. The solvent was evaporated and the residue dissolved in 20 ml of DMF. 200 mg of **L** (MW = 447.43 g/mol, 0.45 mmol) were added and the mixture was refluxed under N_2 for 3 hours. Column chromatography (SiO_2, gradient ACN/KNO_3 aq.) and salt metathesis with NH_4PF_6 afforded 128 mg of complex **p1** (MW = 1161.82 g/mol, 0.11 mmol, 24% yield). ^{1}H (Acetonitrile-d_3, 300 MHz) δH (ppm): 9.17 (d, J = 6 Hz, 2H), 9.11 (d, J = 9 Hz, 2H), 9.04 (s, 2H), 8.67 (d, J = 6 Hz, 2H), 8.23-8.12 (m, 6H), 7.96 (d, J = 6 Hz, 2H), 7.68 (d, J = 6 Hz, 2H), 7.60 (d, J = 9 Hz, 2H), 7.44 (m, 4H), 7.14 (t, J = 6 Hz, 2H), 4.21 (t, J = 6 Hz, 4H), 1.38 (t, J = 6 Hz, 6H) (**Figure S10**). ^{31}P (Acetonitrile-d_3, 121 MHz) δP (ppm): 16.0, -144.6 (sept, *J* = 705 Hz) (**Figure S11**). ESI-MS, m/z: [**p1**]$^+$ calculated for $C_{45}H_{39}N_8O_3PRu$ 872.1926; found 872.13 (55%). [**p1**]$^{2+}$ calculated for $C_{45}H_{39}N_8O_3PRu$ 436.0963; found 436.13 (100%) (**Figure S15**).

The protected compound **p1** was refluxed in 4 M HCl for 48 hours, in order to obtain **1**. ^{1}H (Chloroform-d_1, 300 MHz) δH (ppm): 9.11 (d, J = 6 Hz, 2H), 9.04 (m, 2H), 8.64 (d, J = 9 Hz, 2H), 8.10 (m, 6H), 7.92 (m, 2H), 7.60 (d, J = 6 Hz, 2H), 7.55 (d, J = 9 Hz, 2H), 7.42 (m, 4H), 7.13 (m, 2H) (**Figure S12**). ^{31}P (Chloroform-d_1, 121 MHz) δP (ppm): 10.2, -144.8 (sept, J = 702 Hz) (**Figure S13**). ^{13}C (Acetonitrile-d_3, 300 MHz) δC (ppm): 161.7, 161.0, 160.1, 158.4, 155.6, 154.6, 154.3, 153.3, 149.8, 145.8, 139.1, 138.9, 134.0, 132.0, 130.9, 130.7, 129.6, 129.4, 128.5, 128.0, 127.8, 125.0, 121.6, 119.3 (**Figure S14**). ESI-MS, m/z: $[\mathbf{1}]^{2+}$ calculated for $C_{41}H_{31}N_8O_3PRu$ 408.0650; found 408.0653 (I = 1 x 10^2 counts (%)) (**Figure S17**).

Stationary and time-resolved absorption/emission techniques. Stationary absorption spectra of complexes in solution have been recorded with a JASCO V-560 spectrophotometer, while for the complex **1** grafted onto semiconductor electrodes, were measured between 800 and 400 nm with a JASCO V-570 and a Varian Cary 300 spectrophotometers (bandwidth of 2 nm).

For steady-state luminescence measurements, a Jobin Yvon-Spex Fluoromax P spectrofluorimeter was used, equipped with a Hamamatsu R3896 photomultiplier. The spectra were corrected for photomultiplier response by using a program purchased with the fluorimeter. For the luminescence lifetimes, an Edinburgh OB 900 time-correlated single-photon-counting spectrometer was used. A Hamamatsu PLP 2 laser diode (59 ps pulse width at 408 nm) and/or nitrogen discharge (pulse width 2 ns at 337 nm) were employed as excitation sources.

Transient absorption spectroscopy (TAS) was performed with a previously described apparatus,[50] by using the 532 nm harmonic of a nanosecond *Nd:YAG* laser (*Continuum Surelite II*), with 1.3 kV of supply voltage. Thin films, under open circuit conditions, were oriented at an angle of ca. 45° with respect to the laser beam, defocusing with a plano concave lens and further attenuating with a 50% T neutral filter. Two 532 nm notch filters

prevented laser light from reaching the photomultiplier, while a 420 nm cut-off filter and a 25% T neutral filter attenuated the white light probe beam, preventing a substantial excitation of the exposed semiconductor substrate. In order to obtain a suitable amplification of the oscilloscope traces, with reasonably good S/N ratio, an oscilloscope input resistance of 50 Ω was used. Single wavelength transient traces were further improved by averaging 10 to 30 laser shots at a frequency of 0.2 Hz, imported on a PC and used to construct the transient absorption spectra by means of Origin 8.

Crystal structure determination and refinement. Suitable crystal of **p1** were selected for X-ray analysis (**Figure S18**). Single-crystal X-ray diffraction data are collected on a Bruker APEX II equipped with a CCD area detector and utilizing Mo-Kα radiation (λ = 0.71073 Å) at room temperature. Data were collected and reduced by SMART and SAINT software in the Bruker packages.[51] The structures were solved by direct methods[52] and then refined by least squares refinement on F^2.[53,54] The complete conditions of data collection and structure are given in **Tables S1-S5**. All hydrogens were placed in calculated positions and refined as isotropic with the "riding-model technique". The crystal structure is deposited at the Cambridge Crystallographic Data Center, deposition number CCDC 1474484.

TDDFT calculations. Ground state equilibrium geometry of **p1**, pre-optimized at the semi-empirical PM6 level, were computed at the DFT B3LYP level by using a LANL2DZ basis set. TDDFT/LANL2DZ calculations in the presence of solvent (ACN) described according to the continuum polarisable model (IEFCPM) afforded the ten lowest singlet vertical transitions. Structure and isodensity surfaces (isovalue = 0.004) generation was achieved with Gaussview 5 and Gausssum 2.2. Calculations were carried out with Gaussian 09 A.02[55] by using a multiple core (2 X Intel quad core I7 processors) 64 bit PC running under Linux. The $Ti_{64}O_{128}$ 101 surface slab was optimized in vacuum at the Molecular Mechanics-Universal Force Field level (**Table S8**).

Preparation of electrodes. FTO glass slides 10×8 cm^2 were first cleaned by sonication in Alconox® solution (1 tablespoon in 250 ml of deionized water) for 10 minutes, followed by rinsing with water and by further sonication in 2-propanol for 10 minutes. The slides were finally rinsed with EtOH and dried with warm air. In the case of TiO_2 the semiconductor paste was blade casted onto the active area of the glass (10×3 cm^2) and dried with a warm air stream before high temperature sintering. SnO_2 electrodes were prepared by spin coating the paste at 600 rpm for 6s followed by high speed spinning at 2000 rpm for 20s and after each coating run the film was sintered. The casting of two SnO_2 layer produced the best photoelectrochemical performance.[11] For both TiO_2 and SnO_2 the sintering temperature was set at 450°C for 30 minutes. The slides were cut to obtain single photoanodes having size of 4×1 cm^2 with active area of 1.5 cm^2; these were directly used for the sensitization with **1**.

Electrodes were dipped in 8×10^{-5} M ACN fluid solution of **1**, at 50°C for a couple of hours till saturation of the respective surfaces. The functionalization of **1**/SnO_2 substrates, with an aqueous 2×10^{-3} M IrO_2 nanoparticles (NPs) solution, was performed with two different methods: spin coating 2 times (1000 rpm/min 20s, R.T.),[11] and soaking 15 minutes (R.T.).

Electrochemistry and photoelectrochemistry. Electrochemical measurements in solution were carried out in dry and Ar purged solvents (ACN or DMF), at room temperature with an Autolab multipurpose equipment interfaced to a PC. The working electrode was an Amel glassy carbon (0.08 cm^2) electrode. The counter electrode was a Pt wire, and the pseudo-reference electrode was a silver wire. The reference was set using the redox couple ferrocene/ferrocinium at 395 mV vs. SCE in ACN (internal reference). The concentration in analyte was about 1 mM, unless otherwise stated. 0.1 M $TBAPF_6$ was used as supporting electrolyte. Cyclic voltammograms were obtained at scan rates between 50-500 mV/s and were stated in each case. The criteria for reversibility were the separation of 60 mV between cathodic and anodic peaks, the close to unity ratio of the intensities of the cathodic and

anodic currents, and the constancy of the peak potential on changing scan rate. Electrochemical measurements of sensitized electrodes were carried out on a PGSTAT 30 electrochemical workstation, in a three electrodes configuration using SCE as reference and Pt bead as counter. Cyclic voltammetry of **1** grafted onto TiO_2 and SnO_2 was recorded in ACN/0.1 M $LiClO_4$ at 50 mV/s as scan rate.

Photoelectrochemical experiments were performed at a scan rate of 20 mV/s under AM 1.5 G illumination generated by LOT-Oriel solar simulator equipped with a 420 nm cut-off filter, in order to prevent significant direct bandgap excitation of semiconductors. Different electrolytes were employed, containing sacrificial agents (ACN/LiI and aqueous pH 3 sodium ascorbate) at various concentration (0.1 M, 0.25 M and 0.5 M) for the photoinjection tests. The measurements of **1**/SnO_2 decorated with IrO_2 NPs were performed in aqueous pH 3 0.1 M $NaClO_4$. J-V curves were collected by repeated cycling of the potential between 0.3 V vs. SCE (in sacrificial agent) or 0.5 V vs. SCE (in aqueous $NaClO_4$) and the open circuit potential (V_{oc}) until an overlapping response upon subsequent scan was achieved, indicating the attainment of a stationary state under illumination. Where indicated, the photocurrent density J was obtained by subtraction of the respective electrode dark current. J-V curves under shuttered illumination were acquired by manually chopping the excitation source.

$IPCE = 1.24 \times 10^{-3} (V \cdot m) \frac{J_\lambda (\mu A \cdot cm^{-2})}{\lambda (nm) \times P_\lambda (W \cdot m^{-2})}$ was measured in the same three electrode configuration, under the monochromatic illumination generated by an air cooled Luxtel 175 W Xe lamp coupled to an Applied Photophysics LTD. monochromator. The photocurrent, recorded at the constant potential of 0.3 V vs. SCE, was acquired on an Amel mod.552 potentiostat, in ACN/LiI or aqueous pH 3 ascorbate at various concentration. Incident irradiance was measured with a calibrated silicon photodiode.

ASSOCIATED CONTENT

Supporting Information: Additional photoelectrochemical and spectroscopic data and synthetic schemes are available free of charge via the Internet at http://pubs.acs.org.

AUTHOR INFORMATION

Corresponding Author

*cte@unife.it

*g4s@unife.it

*campagna@unime.it

Present Addresses

† Department of Chemistry and Pharmaceutical Sciences, University of Ferrara, Via Fossato di Mortara 17-19, 44121, Ferrara, Italy.

‡ Department of Chemical, Biological, Pharmaceutical, and Environmental Sciences, University of Messina and Centro Interuniversitario per la Conversione Chimica dell'Energia Solare (SOLAR-CHEM), sezione di Messina, Via Stagno D'Alcontres 31, 98166 Messina, Italy

Author Contributions

The manuscript was written through contributions of all authors. All authors have given approval to the final version of the manuscript.

Funding Sources

Financial support from FIRB Nanosolar project n. RBAP11C58Y and COST Action 1202 (PERSPECT H2O) is gratefully acknowledged.

ACKNOWLEDGMENT

We gratefully acknowledge Dr. Tatiana Bernardi for mass spectroscopy. S.B. is grateful to the European Union's Horizon 2020 Research and Innovation Programme, for the Marie Skłodowska-Curie Individual Fellowship (Grant Agreement No 705723).

REFERENCES

1. J. J. Concepcion, J. W. Jurss, M. K. Brennaman, P. G. Hoertz, A. O. T. Patrocinio, N. Y. Murakami Iha, J. L. Templeton and T. J. Meyer, *Acc. Chem. Res.*, 2009, **42**, 1954-1965.

2. W. J. Youngblood, S.-H. A. Lee, Y. Kobayashi, E. A. Hernandez-Pagan, P. G. Hoertz, T. A. Moore, A. L. Moore, D. Gust and T. E. Mallouk, *J. Am. Chem. Soc.*, 2009, **131**, 926-927.

3. R. Brimblecombe, A. Koo, G. C. Dismukes, G. F. Swiegers and L. Spiccia, *J. Am. Chem. Soc.*, 2010, **132**, 2892-2894.

4. S. Caramori, V. Cristino, R. Argazzi, L. Meda and C. A. Bignozzi, *Inorg. Chem.*, 2010, **49**, 3320-3328.

5. G. F. Moore, J. D. Blakemore, R. L. Milot, J. F. Hull, H.-e. Song, L. Cai, C. A. Schmuttenmaer, R. H. Crabtree and G. W. Brudvig, *Energ. Environ. Sci.*, 2011, **4**, 2389-2392.

6. Y. Zhao, J. R. Swierk, J. D. Megiatto, B. Sherman, W. J. Youngblood, D. Qin, D. M. Lentz, A. L. Moore, T. A. Moore, D. Gust and T. E. Mallouk, *Proc. Natl. Acad. Sci. U.S.A.*, 2012, **109**, 15612-15616.

7. L. Alibabaei, M. K. Brennaman, M. R. Norris, B. Kalanyan, W. Song, M. D. Losego, J. J. Concepcion, R. A. Binstead, G. N. Parsons and T. J. Meyer, *Proc. Natl. Acad. Sci. U.S.A.*, 2013, **110**, 20008-20013.

8. Y. Gao, X. Ding, J. Liu, L. Wang, Z. Lu, L. Li and L. Sun, *J. Am. Chem. Soc.*, 2013, **135**, 4219-4222.

9. J. T. Kirner, J. J. Stracke, B. A. Gregg and R. G. Finke, *ACS Appl. Mater. Interfaces*, 2014, **6**, 13367-13377.

10. L. Alibabaei, B. D. Sherman, M. R. Norris, M. K. Brennaman and T. J. Meyer, *Proc. Natl. Acad. Sci. U.S.A.*, 2015, **112**, 5899-5902.

11. F. Ronconi, Z. Syrgiannis, A. Bonasera, M. Prato, R. Argazzi, S. Caramori, V. Cristino and C. A. Bignozzi, *J. Am. Chem. Soc.*, 2015, **137**, 4630-4633.

12. The biomimetic definition here is based on the similarity of such a mechanism with the natural photosynthetic process, which is considered to be initiated by oxidative photoinduced electron transfer. The anti-biomimetic mechanism, as a consequence, follows an opposite scheme.

13. F. Puntoriero, G. La Ganga, A. Sartorel, M. Carraro, G. Scorrano, M. Bonchio and S. Campagna, *Chem. Comm.*, 2010, **46**, 4725-4727.

14. M. Natali, F. Puntoriero, C. Chiorboli, G. La Ganga, A. Sartorel, M. Bonchio, S. Campagna and F. Scandola, *J. Phys. Chem. C*, 2015, **119**, 2371-2379.

15. In such a system, the excited dendritic antenna is first reduced via photoinduced electron transfer by the molecular catalyst and then the reduced antenna is oxidized back to its ground state by the persulfate sacrificial acceptor. Iteration of the process allows to the molecular catalyst to accumulate holes and finally evolve molecular oxygen from water.[13]

16. A. Kirsch-De Mesmaeker, M. Rochus-Dewitt and J. Nasielski, *J. Phys. Chem.*, 1986, **90**, 6657-6662.

17. D. W. Thompson, C. A. Kelly, F. Farzad and G. J. Meyer, *Langmuir*, 1999, **15**, 650-653.

18. B. V. Bergeron and G. J. Meyer, *J. Phys. Chem. B*, 2003, **107**, 245-254.

19. S. Ardo and G. J. Meyer, *Chem. Soc. Rev.*, 2009, **38**, 115-164.

20. P. Wang, B. Wenger, R. Humphry-Baker, J.-E. Moser, J. Teuscher, W. Kantlehner, J. Mezger, E. V. Stoyanov, S. M. Zakeeruddin and M. Grätzel, *J. Am. Chem. Soc.*, 2005, **127**, 6850-6856.

21. J. T. Hyde, K. Hanson, A. K. Vannucci, A. M. Lapides, L. Alibabaei, M. R. Norris, T. J. Meyer and D. P. Harrison, *ACS Appl. Mater. Interfaces*, 2015, **7**, 9554-9562.

22. F. Puntoriero, A. Sartorel, M. Orlandi, G. La Ganga, S. Serroni, M. Bonchio, F. Scandola and S. Campagna, *Coord. Chem. Rev.*, 2011, **255**, 2594-2601.

23. M.-P. Santoni, G. S. Hanan, B. Hasenknopf, A. Proust, F. Nastasi, S. Serroni and S. Campagna, *Chem. Comm.*, 2011, **47**, 3586-3588.

24. E. A. Medlycott, I. Theobald and G. S. Hanan, *Eur. J. Inorg. Chem.*, 2005, **2005**, 1223-1226.

25. A. Juris, V. Balzani, F. Barigelletti, S. Campagna, P. Belser and A. von Zelewsky, *Coord. Chem. Rev.*, 1988, **84**, 85-277.

26. T. J. Meyer, *Pure Appl. Chem.*, 1986, **58**, 1193-1206.

27. S. Campagna, F. Puntoriero, F. Nastasi, G. Bergamini and V. Balzani, in *Photochemistry and Photophysics of Coordination Compounds I*, eds. V. Balzani and S. Campagna, Springer Berlin Heidelberg, Berlin, Heidelberg, 2007, pp. 117-214.

28. M. I. J. Polson, E. A. Medlycott, G. S. Hanan, L. Mikelsons, N. J. Taylor, M. Watanabe, Y. Tanaka, F. Loiseau, R. Passalacqua and S. Campagna, *Chem. Eur. J.*, 2004, **10**, 3640-3648.

29. H. Zabri, I. Gillaizeau, C. A. Bignozzi, S. Caramori, M.-F. Charlot, J. Cano-Boquera and F. Odobel, *Inorg. Chem.*, 2003, **42**, 6655-6666.

30. J. Lloret Fillol, Z. Codolà, I. Garcia-Bosch, L. Gómez, J. J. Pla and M. Costas, *Nature Chem.*, 2011, **3**, 807-813.

31. M. T. Vagnini, A. L. Smeigh, J. D. Blakemore, S. W. Eaton, N. D. Schley, F. D'Souza, R. H. Crabtree, G. W. Brudvig, D. T. Co and M. R. Wasielewski, *Proc. Natl. Acad. Sci. U.S.A.*, 2012, **109**, 15651-15656.

32. B. M. Klepser and B. M. Bartlett, *J. Am. Chem. Soc.*, 2014, **136**, 1694-1697.

33. A. S. Weingarten, R. V. Kazantsev, L. C. Palmer, M. McClendon, A. R. Koltonow, P. S. SamuelAmanda, D. J. Kiebala, M. R. Wasielewski and S. I. Stupp, *Nature Chem.*, 2014, **6**, 964-970.

34. V. Kunz, V. Stepanenko and F. Wurthner, *Chem. Comm.*, 2015, **51**, 290-293.

35. E_{ox} is the ground state oxidation potential (**Figure 4**), E^{0-0} is the zero-to-zero spectroscopic energy (in eV) that for MLCT emitters is usually approximated to the emission maximum at 77 K (**Table 1**).[25] Other methods to derive the excited-state energy of MLCT states from experimental data are usually acceptable, one is assuming the excited-state energy MLCT state as the energy value corresponding to the 10% intensity of the emission maximum at room temperature, on the blue edge of the emission spectrum. Some small difference is obtained using the two methods, but it does not appreciably change the discussion.

36. Obviously, the reduction potential of the TiO_2 nanoparticles is not well defined, however a value of about -0.70 V vs. SCE can be considered with a fair confidence.[37]

37. A. Di Paola, M. Bellardita, R. Ceccato, L. Palmisano and F. Parrino, *J. Phys. Chem. C*, 2009, **113**, 15166-15174.

38. B. Enright, G. Redmond and D. Fitzmaurice, *J. Phys. Chem.*, 1994, **98**, 6195-6200.

39. The irreversible oxidation process of ascorbate presents several mechanicistic complexities, so its potential is not well-defined. In any case, it is considered to be < +0.7 V vs. SCE.[40]

40. C. Creutz, *Inorg. Chem.*, 1981, **20**, 4449-4452.

41. P. M. Sirimanne and T. Soga, *Sol. Energy Mater. Sol. Cells*, 2003, **80**, 383-389.

42. J. Fielden, J. M. Sumliner, N. Han, Y. V. Geletii, X. Xiang, D. G. Musaev, T. Lian and C. L. Hill, *Chem. Sci.*, 2015, **6**, 5531-5543.

43. Noteworthy, photoinduced electron injection was reported from a supramolecular dinuclear species where the photosensitizer (a Ru(II) polypyridine complex) was covalently-

linked to an electron acceptor (a Rh(III) polypyridine subunit), on its turn connected to TiO_2 nanoparticles.[43] In this system, photoexcitation of the Ru(II) chromophore led to electron transfer to the Rh(III) subunit, and the so-formed charge separated state injected, although with a low efficiency, an electron into the nanoparticles.

44. C. J. Kleverlaan, M. T. Indelli, C. A. Bignozzi, L. Pavanin, F. Scandola, G. M. Hasselman and G. J. Meyer, *J. Am. Chem. Soc.*, 2000, **122**, 2840-2849.

45. J. Wang and G. S. Hanan, *Synlett*, 2005, **2005**, 1251-1254.

46. B. P. Sullivan, J. M. Calvert and T. J. Meyer, *Inorg. Chem.*, 1980, **19**, 1404-1407.

47. A. Orbelli Biroli, F. Tessore, M. Pizzotti, C. Biaggi, R. Ugo, S. Caramori, A. Aliprandi, C. A. Bignozzi, F. De Angelis, G. Giorgi, E. Licandro and E. Longhi, *J. Phys. Chem. C*, 2011, **115**, 23170-23182.

487. M. Hara, C. C. Waraksa, J. T. Lean, B. A. Lewis and T. E. Mallouk, *J. Phys. Chem. A*, 2000, **104**, 5275-5280.

49. V. Spampinato, N. Tuccitto, S. Quici, V. Calabrese, G. Marletta, A. Torrisi and A. Licciardello, *Langmuir*, 2010, **26**, 8400-8406.

50. M. Mba, M. D'Acunzo, P. Salice, T. Carofiglio, M. Maggini, S. Caramori, A. Campana, A. Aliprandi, R. Argazzi, S. Carli and C. A. Bignozzi, *J. Phys. Chem. C*, 2013, **117**, 19885-19896.

51. Bruker AXS Inc., SMART (Version 5.060) and SAINT (Version 6.02): Madison, Wisconsin, USA, **1999**.

52. M. C. Burla, R. Caliandro, M. Camalli, B. Carrozzini, G. L. Cascarano, L. De Caro, C. Giacovazzo, G. Polidori and R. Spagna, *J. Appl. Cryst.*, 2005, **38**, 381-388.

53. G. M. Sheldrick; SHELXL97, Program for Crystal Structure Refinement: University of Göttingen, Germany, **1997**.

54. Bruker Analytical X-ray Inc., SHELXT LN, Version 5.10 Madison, WI, USA, **1998**.

55. M. J. Frisch, G. W. Trucks, H. B. Schlegel, G. E. Scuseria, M. A. Robb, J. R. Cheeseman, G. Scalmani, V. Barone, B. Mennucci, G. A. Petersson, H. Nakatsuji, M. Caricato, X. Li, H. P. Hratchian, A. F. Izmaylov, J. Bloino, G. Zheng, J. L. Sonnenberg, M. Hada, M. Ehara, K. Toyota, R. Fukuda, J. Hasegawa, M. Ishida, T. Nakajima, Y. Honda, O. Kitao, H. Nakai, T. Vreven, J. A. Montgomery Jr., J. E. Peralta, F. Ogliaro, M. J. Bearpark, J. Heyd, E. N. Brothers, K. N. Kudin, V. N. Staroverov, R. Kobayashi, J. Normand, K. Raghavachari, A. P. Rendell, J. C. Burant, S. S. Iyengar, J. Tomasi, M. Cossi, N. Rega, N. J. Millam, M. Klene, J. E. Knox, J. B. Cross, V. Bakken, C. Adamo, J. Jaramillo, R. Gomperts, R. E. Stratmann, O. Yazyev, A. J. Austin, R. Cammi, C. Pomelli, J. W. Ochterski, R. L. Martin, K. Morokuma, V. G. Zakrzewski, G. A. Voth, P. Salvador, J. J. Dannenberg, S. Dapprich, A. D. Daniels, Ö. Farkas, J. B. Foresman, J. V. Ortiz, J. Cioslowski and D. J. Fox, 2009.

Table of Contents Graphic and Synopsis

The charge transfer dynamics involving a new Ru(II) polypyridine complex, adsorbed on mesoporous TiO_2 photoanodes, has been studied under 1 sun illumination. The increase of the photocurrents from 0.2 mA/cm^2, in acetonitrile with 0.1 M LiI, to 0.7 mA/cm^2, when 0.1 M aqueous pH 3 sodium ascorbate is used as sacrificial donor, has been rationalized with a modification of the charge injection mechanism to the semiconductor, supported by transient absorption spectroscopy experiments.

A table of contents entry: graphic maximum size 8 cm x 4 cm and one sentence of text, maximum 20 words, highlighting the novelty of the work